Available online at www.sciencedirect.com
SCIENCE DIRECT®

Journal of the European Ceramic Society 24 (2004) 877–885

www.elsevier.com/locate/jeurceramsoc

Influence of carbon fibre content on the processing and tribological properties of silicon nitride/carbon fibre composites

Hideki Hyuga[a,*], Mark I. Jones[b], Kiyoshi Hirao[b], Yukihiko Yamauchi[b]

[a]*Fine Ceramics Research Association, 2268-1 Shimo-shidami, Nagoya 463-8687, Japan*
[b]*Synergy Materials Research Center, AIST, 2268-1 Shimo-shidami, Nagoya 463-8687, Japan*

Received 9 January 2003; received in revised form 20 March 2003; accepted 6 April 2003

Abstract

Si_3N_4/carbon fibre composites have been fabricated, and the effect of fibre content on the tribological properties was investigated under dry sliding conditions. The friction coefficient of the composites was around 30% of that of a monolithic Si_3N_4 composite. A fibre content of 5 vol.% was sufficient to maintain a graphite interface during the sliding tests, such that the friction coefficient did not decrease further with increasing graphite fibre content above this level. The carbon fibre content was effective for maintaining a low friction coefficient throughout the duration of the experiment.

Keywords: Carbon fibre; Composites; Fibres; Si_3N_4; Wear resistance; Wear parts

1. Introduction

Ceramic materials exhibit properties that make them suitable candidates for a number of industrial applications. In the field of machinery industries, they are expected to be used where the tribological environment is severe, such as under high normal pressures and corrosive environments.[1–3] In particular, there is the possibility of using ceramics in tribological applications under non-lubricated or marginally lubricated sliding contacts.

Compared with other engineering ceramics, silicon nitride has superior mechanical properties, with high fracture strength and fracture toughness. In tribological applications, Si_3N_4 ceramics have been used as the ball component of bearing systems under lubricated conditions. However, the sliding contact of Si_3N_4–Si_3N_4 self-mated tribopairs under dry conditions produces a high friction coefficient and high wear rate because the abrasive wear is affected by the intrinsic brittle nature of ceramics.[4,5] Therefore, many attempts have been carried out to produce Si_3N_4-based ceramics with a solid lubrication function, and many researchers have reported self-lubricating materials such as composites including graphite, boron nitride, and molybdenum.[6–9] Amongst these materials, graphite possesses one of the highest solid lubricating functions. However, technical problems arise during the fabrication of ceramic graphite composites, since the fine graphite powder employed is difficult to mix with the raw ceramic powder due to its hydrophobic nature, and results in adhesion to the balls and pot used for the ball milling. Many researchers have also reported that the tribological properties of carbon based materials such as graphite, DLC and cluster diamond make them promising as low friction materials.[10–13] However, simply coating of the bulk material does not provide the reliability required for use in severe conditions. Jahanmir et al. succeeded in producing self-lubricating materials by adding carbon incorporated $NiCl_2$ to a Si_3N_4 matrix in which holes had been drilled by a machining process.[14] In graphite materials, there is little work reporting on the solid lubrication properties of ceramic/carbon fibre composites. It has been reported that the solid-lubrication effect of ceramic/carbon composites is not sufficient to allow their use in tribological applications under dry sliding conditions. Blau et al. reported that under dry sliding conditions against a stainless steel counter body, a Si_3N_4 ceramic/carbon fibre composite did not produce any beneficial lubricating

* Corresponding author.
E-mail address: h-hyuga@aist.go.jp (H. Hyuga).

0955-2219/03/$ - see front matter © 2003 Elsevier Ltd. All rights reserved.
doi:10.1016/S0955-2219(03)00263-2

effect when compared with the results of the matrix material alone.[15] It was suggested that this was because the formation of a graphitic lubricating film on the surface of the counterbody did not occur, due to the inherent properties of the fibre employed. The properties of carbon fibres, in particular the elastic modulus, are determined by the degree of texturing of the graphite bonding layers and by the amount of graphitic bonding in the carbon fibre composition. Our group has recently shown that fibres with a high degree of orientation and high graphite content were effective for decreasing the friction coefficient.[16] In this study, Si_3N_4/carbon fibre composites have been fabricated with different fibre contents, and the effect of fibre content on the tribological properties was investigated under dry sliding conditions.

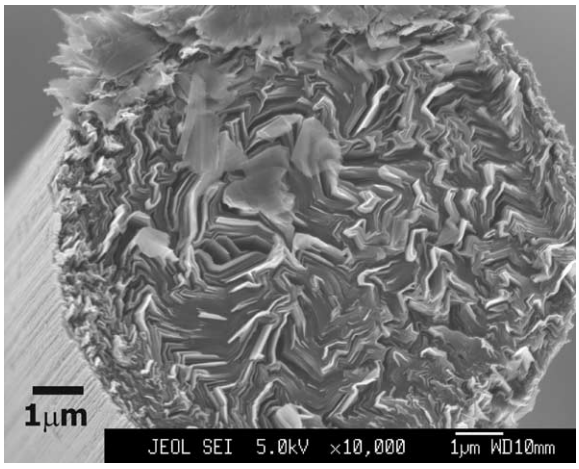

Fig. 1. Cross section of the carbon fibre used in this study.

2. Experimental procedure

2.1. Sample preparation

Yttrium oxide (RU-P grade, Shin-etsu chem. Co. Ltd., Tokyo, Japan) and aluminium oxide (AKP-50, Sumitomo Kagaku Co. Ltd., Tokyo, Japan) powders were added to silicon nitride (ESP grade, Ube Industries Ltd., Tokyo, Japan), powder as sintering additives. The composition of the starting powders was 93 mass% Si_3N_4, 2 mass% Al_2O_3 and 5 mass% Y_2O_3. The raw powder was homogeneously mixed by ball milling and then dried. Following sieving of the dried powders, they were mixed with 1–20 vol.% of the respective carbon fibres (XN-100; Nippon graphite fiber co. Ltd., Tokyo, Japan) using planetary ball milling. The composite powders were hot-pressed at 1950 °C for 2 h at 30 MPa pressure in a 900 kPa nitrogen atmosphere. Table 1 shows the properties of the fibres used in this study, and cross sections of the fibres observed by scanning electron microscopy (SEM) are shown in Fig. 1.

2.2. Characterization of the specimens

The sintered bodies were cut, ground and crushed before phase analysis by XRD. The densities of the machined specimens were measured using the Archimedes method in distilled water. The size and distribution of the fibres in the specimens were observed by optical microscopy.

Table 1
Properties of the carbon fibre used in this study

	XN-100[a]
Tensile modulus (GPa)	1000
Tensile strength (GPa)	3.5
Densilty (g/cm^3)	2.22
Filament Diameter (μm)	10
Base material	Pitch

[a] Product name by Nippon graphite fiber Co. Ltd.

For bending strength measurements, test bars with dimensions of 3 mm×4 mm×40 mm were machined from the sintered body and polished on the tensile face. Four point bending strength measurements were conducted with an inner span of 10 mm, outer span of 30 mm, and a crosshead speed of 0.5 mm min^{-1}. Fracture toughness (K_{1C}) was determined by the single etched notched beam (SEPB) method with a span of 18 mm.[17] In both cases the results are presented as the average of a minimum of five separate measurements.

2.3. Friction tests

Friction behaviour was evaluated by unlubricated ball-on-disk experiments, carried out under various loads against a polished commercial Si_3N_4 ball with diameter of 9.525 mm (Nihon ceratec Co. Ltd., Miyagi, Japan). The Si_3N_4 sintered bodies were machined into 30 mm×27 mm×5 mm as the plate specimens. Wear tests were carried out under dry conditions in air in order to eliminate any lubricating effect from other sources. Temperature and humidity were kept constant at 25±3 °C, 25±5% relative humidity, respectively. Sliding conditions were set at 20 mm sliding diameter, 0.18 m s^{-1} sliding speed and 108 m sliding distance. The friction force and applied force were measured continuously during each test.

Wear volumes of the worn specimens were evaluated using a roughness tester and optical microscope. For the worn plate specimen, the cross sectional area of the worn track was taken as the average of that measured at four separate locations. The worn volume, V_{plate} was calculated according to the following equation, and in all cases, the values reported are the average of five different tests;

$$V_{plate} = 2\pi R((S_1 + S_2 + S_3 + S_4)/4) \quad (1)$$

where R and S are the sliding radius and cross section area of the worn track.

For the worn ball specimen, the diameter of the worn circle was measured at four equi-distant locations. The worn volume, V_{ball} was calculated according to the following equation, and in all cases, the values reported are the average of five different tests the same as for the case of V_{plate};

$$V_{ball} = \pi A^3 B/32D \quad (2)$$

where A and B are the longer and shorter diameter of the worn area of the ball, and D is the ball diameter.[18,19] The surface of the specimens after wear tests was observed by scanning electron microscopy and optical microscopy to clarify the worn behaviour.

Raman spectroscopy was carried out on the surfaces both before and after wear tests. An Ar laser was used giving a monochromatic blue light of 488 nm at a power of 0.3 mW. A charged coupled device (CCD) camera was used to collect the Raman spectra in the range from 1100 to 1800 nm. The graphite ratio on the worn surface was calculated from the carbon peaks observed in the spectra.[20,21]

3. Results and discussions

3.1. Microstructure and mechanical properties

Sintered specimens with carbon fibre contents less than 20 vol.% were fully dense (>99% theoretical density). For the 20 vol.% carbon fibre addition, the density of the specimens was 95%.

Fig. 2 shows optical microscope images of the Si_3N_4/carbon fibre composites with the different fibre content. Homogeneously dispersed carbon fibres were observed in all specimens. Image analysis results indicated that the length of the fibres in all the specimens was almost the same at about 150 μm. XRD analysis showed that for less than 20 vol.% carbon fibre content the only crystalline phases present in the composites were β-Si_3N4 and graphite, with no SiC phases being detectable. For the 20 vol.% carbon fibre content, SiC and $Y_2Si_3O_3N_4$ phases were detectable. The intensity of the (002) graphite peak increased with increasing carbon fibre contents (Fig. 3).

The reaction between carbon and Si_3N_4 can be expressed as,

$$Si_3N_4 + 3C \Longleftrightarrow 3SiC + 2N_2 \quad (3)$$

This reversible reaction was found to proceed to the right under the conditions of 0.9 MPa nitrogen pressure and sintering temperatures over 1700 °C.[22] Reactions between carbon and oxides occurs due to the sintering additives and the silica on the surface on the silicon nitride powder result in the formation of carbon monoxide gas. If densification is fast it is difficult for the carbon monoxide and nitrogen gas to move away freely along the grain boundary, and the only method of gas diffusion is by solid-state diffusion, which is extremely slow. The lack of detection of phases such as SiC up to 10 vol.% carbon fibre content, suggests that under these sintering conditions the densification was sufficiently rapid to so as to prevent their formation. On the other hand, for the 20 vol.% carbon fibre content, densification was slow such that the above reaction could take place. The lower density of the 20 vol.% carbon fibre addition is attributed to the fact that the SiC reaction phase inhibited the densification. In addition to the earlier reaction, the $Y_2Si_3O_3N_4$ phase, which is produced under lower oxygen conditions,[23] was detected by XRD, indicating that oxygen in the composite was removed by reaction with the carbon fibres. Fig. 4 shows the dependence of carbon fibre content on the fracture strength and toughness of the composites.

The fracture strength decreased with increasing carbon fibre content. The fracture behaviours of all the composites indicated brittle fracture. The fracture strength decreased drastically with only 1 vol.% carbon fibre addition and continued to decrease with increasing carbon fibre content. This behaviour was caused by the carbon fibres acting as the origin of fracture, even with additions of only 1 vol.%. As the volume fraction of fibres increased the size of the fracture origin is considered to increase due to interaction with neighbouring fibres leading to the continuous decrease in strength observed with increasing fibre content.

On the other hand, fracture toughness was increased up to 11 MPa $m^{1/2}$ in the case of 1 vol.% carbon fibre content and the fracture toughness of all the composites was significantly higher than that of the monolithic silicon nitride. SEM images of the fractured surface of the composites are shown in Fig. 5. Fibre pull out was observed as reported by many researchers[24,25] for ceramics/fibre composites, and this mechanism was responsible for the toughening effects of the Si_3N_4/carbon short fibre composite.

3.2. Tribological properties

Fig. 6 shows the variation of friction coefficient with sliding distance for the carbon fibre composites. In the case of monolithic Si_3N_4, the initial friction coefficient indicated higher values, which were maintained in the steady state. On the other hand, although the initial friction coefficient of the Si_3N_4/carbon fibre composites also indicated high values, it gradually decreased and was in the range of 0.2–0.3 for every sample. For the specimens with more than 5 vol.% carbon fibre addition the value remained low throughout the test. In the case

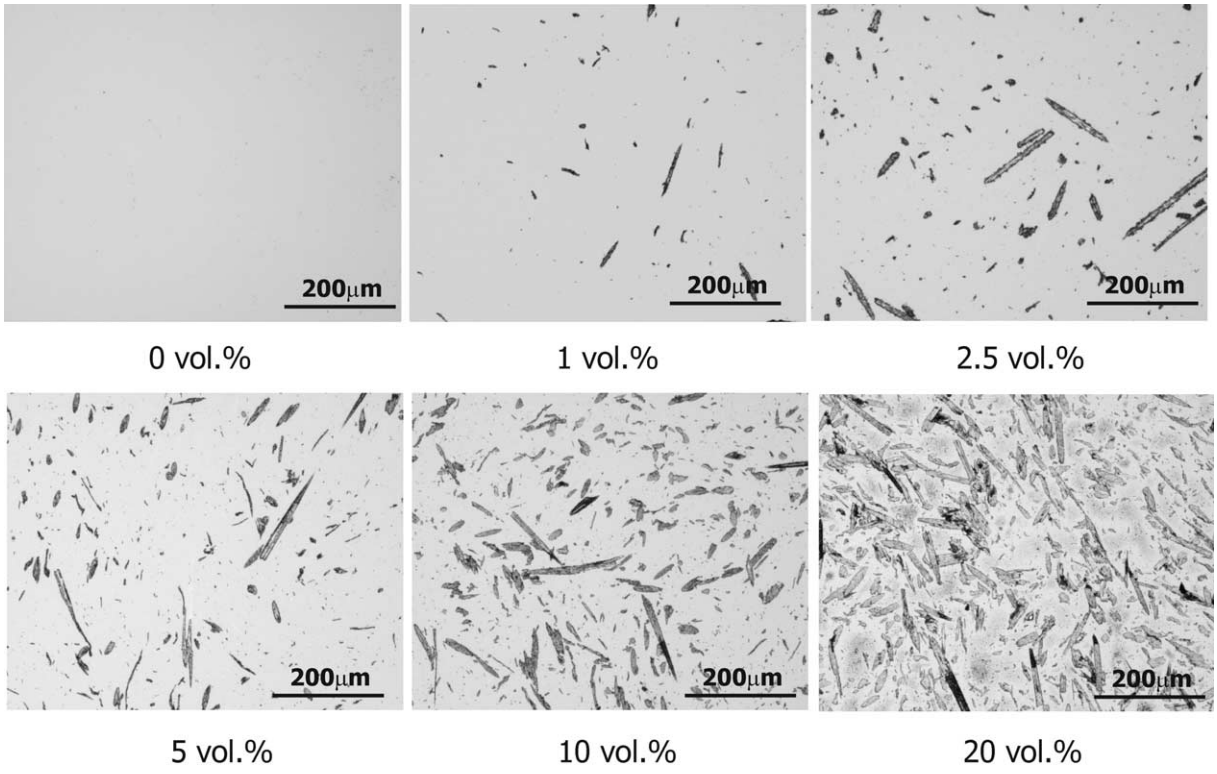

Fig. 2. Optical microscope images of the Si_3N_4/carbon fibre composites with different amount of carbon fibre volume fraction.

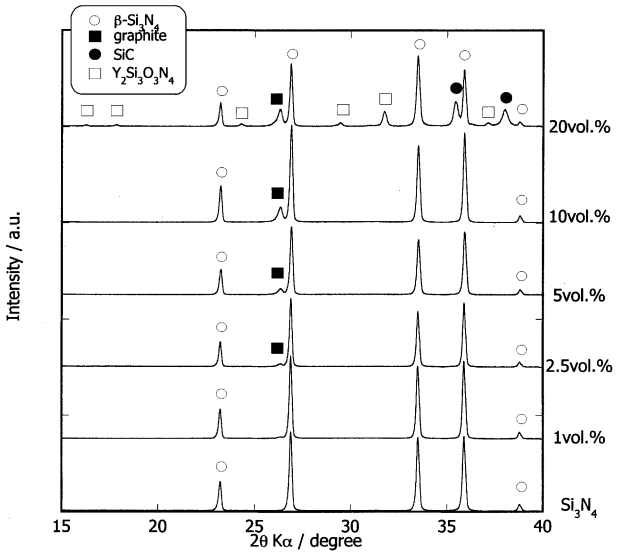

Fig. 3. X-ray diffraction patterns of the various Si_3N_4/carbon fibre composites.

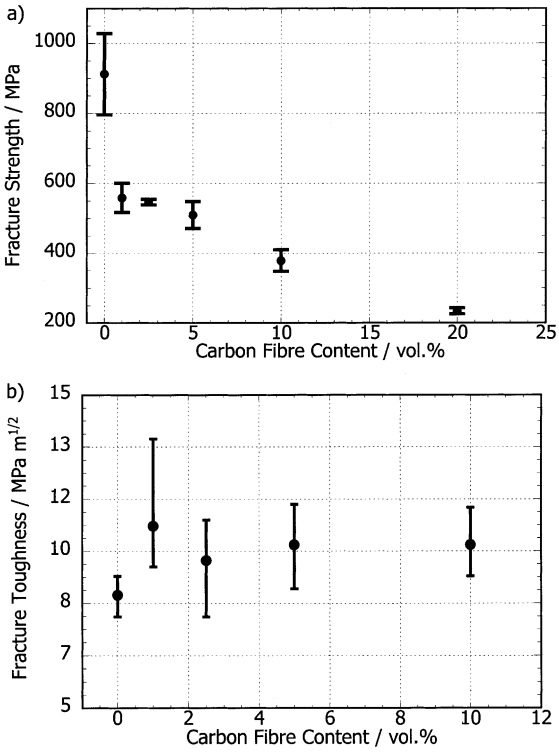

Fig. 4. The influence of carbon fibre content on the fracture strength (a) and fracture toughness (b) of the composites.

of low carbon fibre content, the friction coefficient gradually increased to values similar to that of the monolithic Si_3N_4.

Fig. 7 shows the relationship between carbon fibre content and average friction coefficient during wear, neglecting the initial running in period. The friction coefficient decreased with increasing fibre content up to 5 vol.%, then showed no change for higher contents. For those composites with fibre content greater than 5 vol.%, the friction coefficient indicated constant values of around 0.2, which is about 25% of that of monolithic Si_3N_4.

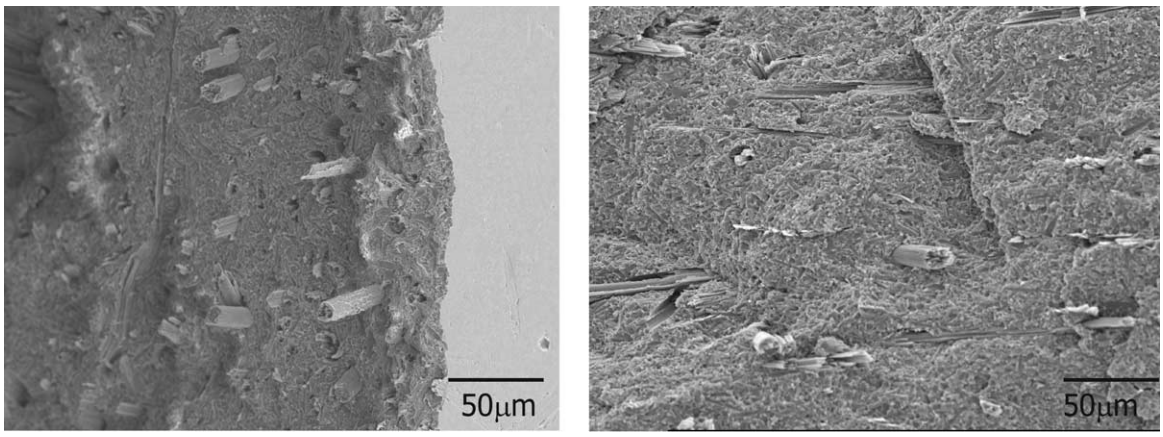

Fig. 5. Fracture surfaces of the Si_3N_4/5 vol.% carbon fibre composites after bending tests.

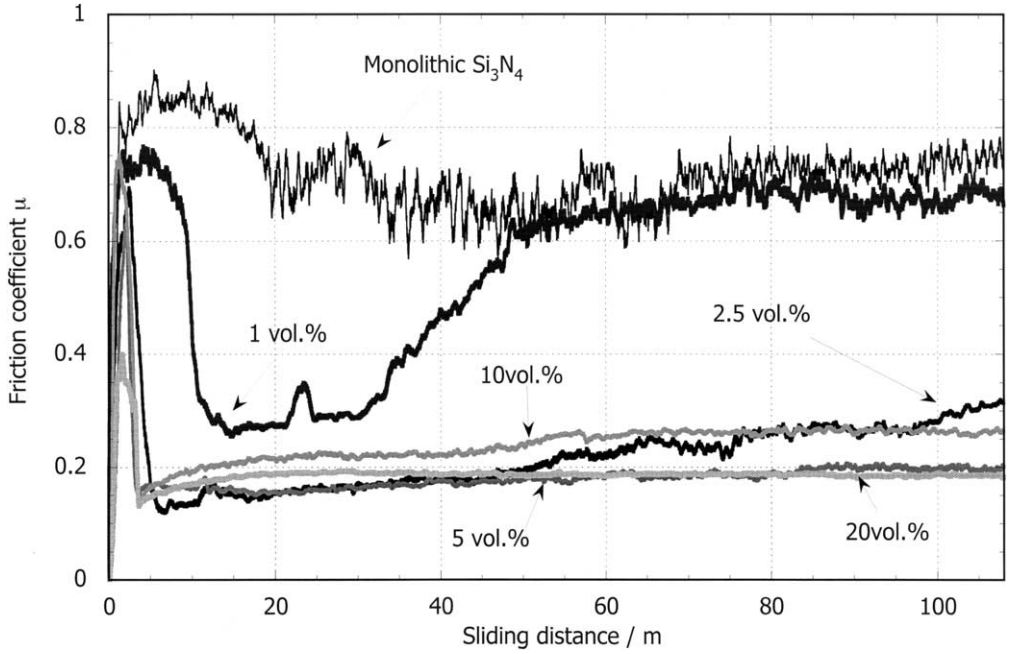

Fig. 6. The variation of friction coefficient with sliding distance for the carbon fibre composites.

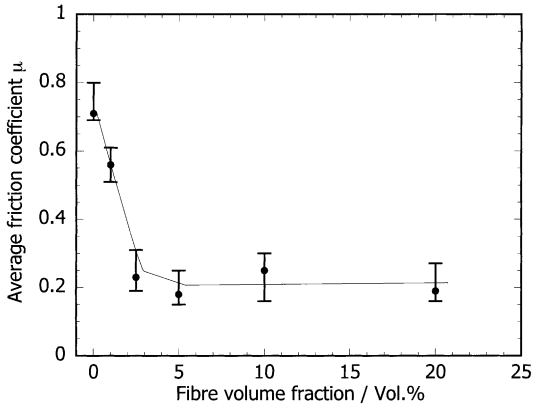

Fig. 7. The relationship between carbon fibre content and average friction coefficient.

Fig. 8 shows the relationship between specific wear rate of the disks and the carbon fibre content. The minimum value of specific wear rate was observed for the sample with 1 vol.% carbon fibre addition. However, the wear rate increased for higher fibre contents.

Fig. 9 shows worn tracks of the disks. The worn track of monolithic Si_3N_4 showed a rough surface with fine crushed debris. On the other hand, for the composite specimens, the graphite fibres were preferentially worn in all cases. In addition the worn tracks were covered with adhesive debris with a smooth appearance, which may have consisted mainly of SiO_2 formed by tribo-chemical reaction[26] and graphite. For composites with more than 10 vol.% carbon fibre additions, the matrix

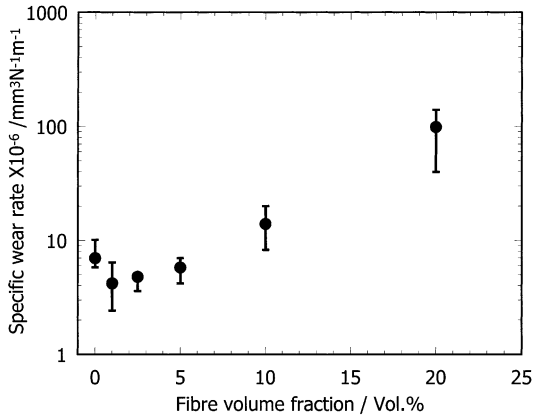

Fig. 8. The relationship between specific wear rate of the disks and the carbon fibre volume fraction.

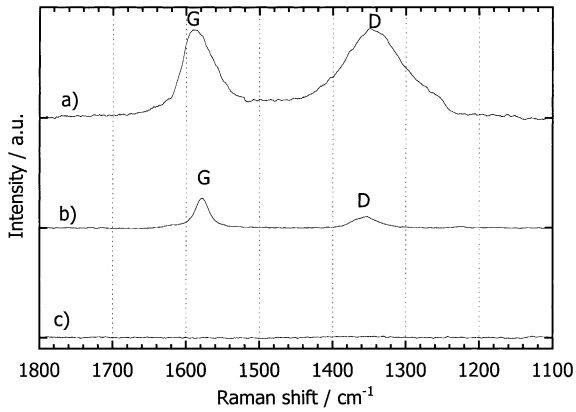

Fig. 10. Raman spectra of the disk of before and after wear test (a) after wear, (b before wear, (c monolithic Si_3N_4.

of the composite inside the worn surface was fractured during the sliding test.

Fig. 10 shows the Raman spectra of the surface of the composite with 5 vol.% carbon fibre addition before and after wear test.

Hexagonal graphite has a crystal structure built up of flat layers in which the trivalent carbon atoms occupy the lattice sites of a two-dimensional honeycomb network. On the other hand, amorphous carbon-based materials do not have such a honeycomb structure and the carbon atoms inside the material have various valences. Raman spectroscopy is a useful technique for determining the carbon structure. In addition to the hexagonal graphite ordered peak (about 1580 cm^{-1}) typical of the graphite crystal, carbon materials in general (especially carbon fibre) present a disordered peak (about 1350 cm^{-1}) in the first order Raman spectrum as a consequence of the relaxation of selection rules due to the existence of structural disorder.[27–29] Both disorder and graphite structure peaks were increased on the worn surface, and the graphite ratio was decreased compared with the ratio before the wear test. These results indicated that the graphite fibres inside the composite were supplied to the worn surface as a result of partial fracture followed by grain dropping during the wear test and acted as solid lubrication with adhesion on the surface

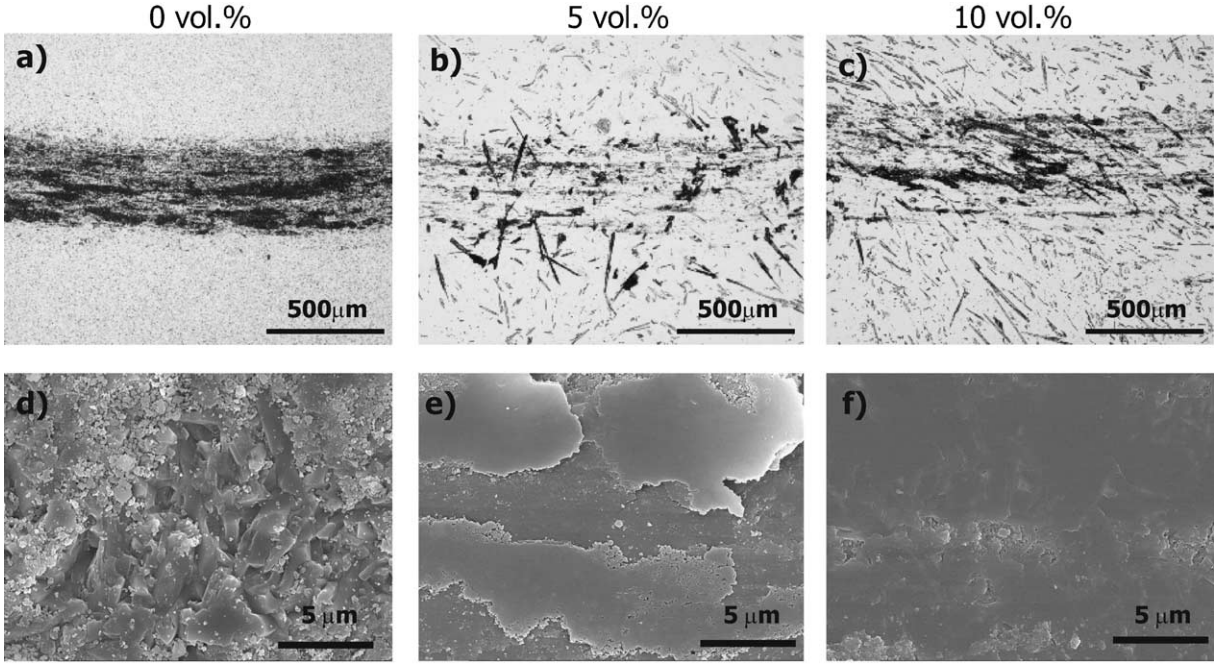

Fig. 9. Optical (a,b,c) and SEM (d,e,f) images of the worn surfaces of the Si_3N_4/carbon fibre composites with different amount of carbon fibre volume fraction (a,d) monolithic Si3N4; (b,e) 5 vol.% carbon fibre addition; (c,f) 10 vol.% carbon fibre addition. (a–c) Were images by optical microscope and (d–f) were images by SEM.

depleting the graphite layer structure of the carbon fibres. The bonding energy between crystal layers of graphite is weak,[30] such that slip between crystal layers is assumed to be one of the dominant mechanisms of low-friction sliding. The friction coefficient of graphite has been reported to be <0.1 up to 600 °C under dry conditions.[31] To clarify the graphite lubrication effects, the friction coefficient of a Si_3N_4 dipped in graphite powder was evaluated under the same conditions and indicated a value of 0.15. The friction coefficient of the fabricated composites indicated almost the same values as that of the graphite dipped sample. It was considered from the values of friction coefficient of these composites that the sliding condition was almost graphite–graphite contact. The friction coefficient did not decrease with further increasing of the graphite content above the 5 vol.% graphite fibre addition because the graphitic content of this composite was sufficient to maintain the graphite–graphite contact. The solid lubrication effect of the graphite fibres restricted the increasing of Hertzian stress contact during sliding conditions. Calculated values of maximum tensile stress values are shown in Table 2. The Hertzian stress was obviously decreased owing to the lower friction coefficient. The abrasive wear mechanism of Si_3N_4 ceramics is considered to be caused by grinding or ploughing of the surface by grains that have been previously removed due to high Hertzian stresses. This removal of grains occurs readily due to the weaker grain boundary phase, which is always present due to addition of sintering additives.[5,32]

In the composites, the solid lubrication effects restricted the stress concentration in the real contact area and the wear mode was not changed to abrasive wear, thus resulting in smooth wear surfaces. However, although fracturing of the matrix did not occur, the partial fracturing and dropping of the carbon fibres contributed to the worn volume so that the specific wear rate was not drastically reduced. As a result, it was considered that the fabricated composites with over 10 vol.% carbon fibre content did not have higher wear resistance compared with monolithic Si_3N_4.

The 1 vol.% carbon addition had the highest wear resistance despite the fact that its friction coefficient was not the lowest. The increase in friction coefficient of this sample with sliding distance was due to the depletion of the graphite structure of the carbon fibres, thus eliminating the graphite lubrication effect. However, the fact that a carbon film was maintained on some areas of the worn disk meant that direct Si_3N_4–Si_3N_4 contact between the ball and disk was restricted. Under these conditions, the preferential removal of the grain boundary was restrained and the wear rate remained low.

Fig. 11 shows the relationship between specific wear rate of the ball and carbon fibre content. Specific wear rate of the ball as the counterbody was decreased for the specimens with more than 5 vol.% carbon fibre additions.

Table 2
Calculation results of Hertzian stress in this wear test condition

		Contact area radius (μm)	Maximum compressive stress (MPa)	Maximum tensile stress (static) (MPa)	Maximum tensile stress (in sliding) (MPa)
Si_3N_4/5 vol.% carbon fibre composite	4.9 N	51	600	170	440 ($\mu=0.2$)
Si_3N_4	4.9 N	48	670	150	1400 ($\mu=0.7$)

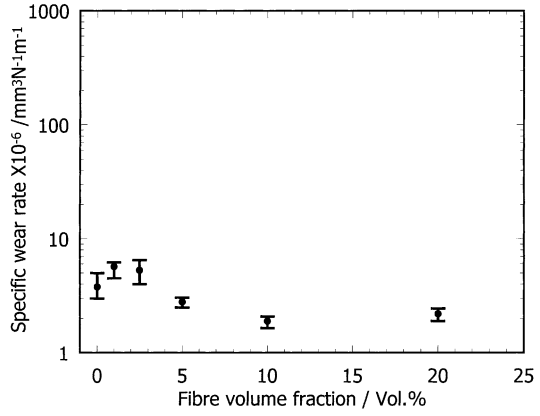

Fig. 11. The relationship between specific wear rate of the balls and the carbon fibre volume fraction.

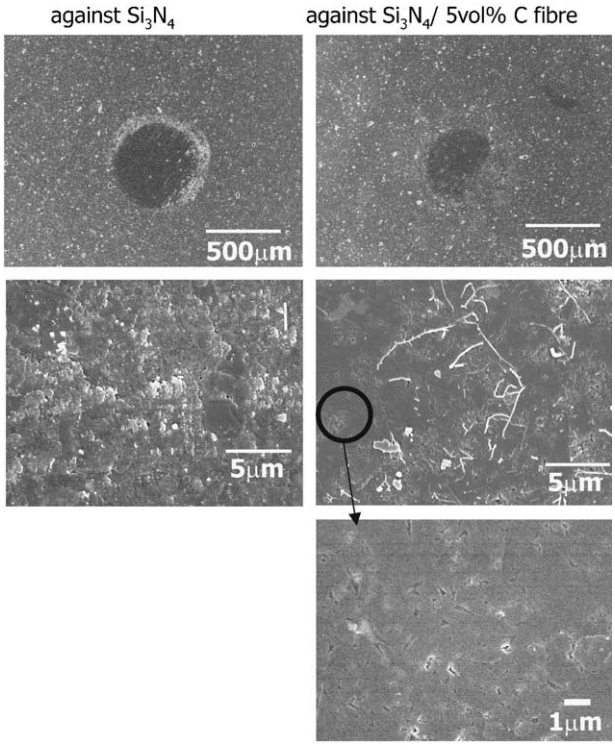

Fig. 12. SEM images of the worn surfaces of the balls.

Fig. 12 shows SEM images of worn surfaces of the balls. In the case of the worn surfaces against conventional Si_3N_4 disks, the surface contained areas where grain dropping had occurred during the wear. On the other hand, the surface of the ball worn against the Si_3N_4/5 vol.% carbon fibre composite was very smooth compared with the conventional Si_3N_4 and adherent debris was observed in some areas. The morphology of this debris was not particle-like, but rather fibrous debris. The individual fibrous debris was several tens of nanometres in diameter and a few microns in length. This type of debris was formed by mechano–chemical reaction due to the humidity in the air during the wear test.[33] Moreover, on the smooth parts of the wear surface, no scratches or cracks caused by abrasive wear conditions could be observed. The graphite lubrication effect restricted the transition of the wear mode from adhesion to abrasive for the balls and also provided the high wear resistance against the counterbody.

4. Conclusion

1. Si_3N_4/carbon short fibre composites were fabricated using high tensile modulus and high-layered orientation graphite fibres. The obtained composites had high fracture toughness and high tribological performance.
2. The friction coefficient of these composites was around 30% of that of a monolithic Si_3N_4 composite under unlubricated conditions. A fibre content of 5 vol.% was sufficient to maintain a graphite interface during the sliding tests, such that the friction coefficient did not decrease further with increasing graphite fibre content above this level.

Acknowledgements

This work has been supported by METI, Japan, as part of the Synergy Ceramics Project. Part of the work has been supported by NEDO. The authors are members of the Joint Research Consortium of Synergy Ceramics.

References

1. Kitamura, K., Takebayashi, H., Ikeda M. and Percoulis, H. M. Development of Ceramic Cam Roller Follower for Engine Application, SAE paper, 1997 (No. 972774).
2. Tanimoto, K., Kajihara K., and Yanai, K. Hybrid Ceramic Ball Bearings for Turbochargers, SAE paper, 2000 (No. 2000-01-1339).
3. Wang, L., Snidle, R. W. and Gu, L., Rolling contact silicon nitride bearing technology: a review of recent research. *Wear*, 2000, **239**, 176–188.
4. Andersson, P. and Holmberg, K., Limitation on the use of ceramics in unlubricated sliding application due to transfer layer formation. *Wear*, 1994, **175**, 1–8.
5. Hyuga, H., Sakaguchi, S., Hirao, K., Yamauchi, Y. and Kanzaki, S., Influence of microstructure and grain boundary phase on tribological properties of Si_3N_4 ceramics. *Ceramic Engineering and Science Proceedings*, 2001, **22**(3), 197–202.
6. Saito, T., Hosoe, T. and Honda, F., Chemical wear of sintered Si_3N_4, hBN and Si_3N_4–hBN composites by water lubrication. *Wear*, 2001, **247**, 223–230.
7. Skopp, A. and Woydt, M., Ceramic–ceramic composite materials with improved friction and wear properties. *Tribo. Int*., 1992, **25**, 61–70.
8. Iizuka, T., Murao, T., Yamamoto, H. and Kita, H., Fabrication and wear behavior of Mo_5Si_3 particles reinforced Si_3N_4 composite. *J. Ceram. Soc. Jpn*, 2001, **109**, 699–703 (in Japanese).
9. Liu, H. W. and Xue, Q., The tribological properties of TZP-graphite self-lubricating ceramics. *Wear*, 1996, **198**, 143–149.
10. Savage, R. H., Graphite lubrication. *J. Appl. Phys*, 1948, **19**(1), 1–10.
11. Holmberg, K., Matthews, A. and Ronkainen, H., Coatings tribology—contact mechanisms and surface design. *Tribo. Int*., 1998, **31**, 107–120.
12. Nakayama, N., Mayuzumi, M., Hanada, K., Sano, T., Tominaga, R. and Takeishi, H., Thin-film forming of cluster diamond-dispersed aluminum composite by dynamic compaction. *Key Eng. Mat*., 2000, **177–1: Part 1&2**, 787–792.
13. Khurshudov, A. G., Olsson, M. and Kato, K., Tribology of unlubricated sliding contact of ceramic materials and amorphous carbon. *Wear*, 1997, **205**, 101–111.
14. Gangopadhyay, A. and Jahanmir, S., Friction and wear characteristics of silicon nitride–graphite and alumina–graphite composites. *Tibol. Trans*., 1991, **34**(2), 257–265.
15. Blau, P. J., Dumont, B., Braski, D. N., Jenkins, T., Zanoria, E. S. and Long, M. C., Reciprocating friction and wear behaviour of a ceramic–matrix graphite composite for possible use in diesel engine valve guides. *Wear*, 1999, **225–229**, 1338–1449.
16. Hyuga, H., Hirao, K., Jones, M. I. and Yamauchi, Y., Processing and tribological properties of Si_3N_4/carbon short fiber composites. *J. Am. Ceram. Soc*. (in press).
17. Nose, T. and Fujii, T., Evaluation of fracture-toughness for ceramic materials by a single-edge-precracked-beam method. *J. Am. Ceram. Soc*., 1988, **71**(5), 328–333.
18. Krell, A. and Klaffke, D., Effects of grain size and humidity on fretting wear in fine-grained alumina, Al_2O_3/TiC, and zirconia. *J. Am. Ceram. Soc*., 1996, **79**(5), 1139–1146.
19. Japanese Industrial Standard (JIS), *Testing Method for Wear Resistance of High Performance Ceramics by Ball-on-Disk Method*. 1993 (R1613).
20. Montes-Moran, M. A. and Young, R. J., Raman spectroscopy study of HM carbon fibres: effect of plasma treatment on the interfacial properties of single fibre/epoxy composites Part I: Fibre characterisation. *Carbon*, 2002, **40**, 845–855.
21. Endo, M., Kim, C., Karaki, T., Kasai, T., Matthews, M. J., Brown, S. D. M., Dresselhaus, M. S., Tamaki, T. and Nishimura, Y., structural characterization of milled mesophase pitch-based carbon fibers. *Carbon*, 1998, **36**(11), 1633–1641.
22. Seifert, H. J., Peng, J., Lukas, H. L. and Aldinger, F., Phase equilibria and thermal analysis of Si–C–N ceramics. *J. Alloys Comp*., 2001, **320**, 251–261.
23. Gauckler, L. J., Hohnke, H. and Tien, T. Y., System Si_3N_4–SiO_2–Y_2O_3. *J. Am. Ceram. Soc*., 1980, **63**(1), 35–37.
24. Suzuki, T. and Umehara, H., Pitch-based carbon fiber microstructure and texture and compatibility with aluminum coated using chemical vapor deposition. *Carbon*, 1999, **37**, 47–59.

25. Nakano, K., Kamiya, A., Nishio, Y., Imura, T. and Chou, T. W., Fabrication and characterization of three-dimensional carbon fiber reinforced silicon carbide and silicon nitride composite. *J. Am. Ceram. Soc.*, 1995, **78**(10), 2811–2814.
26. Dong, X. and Jahanmir, S., Wear transition diagram for silicon-nitride. *Wear*, 1993, **165**(2), 169–180.
27. Tuinstra, F. and Koenig, J. L., Raman spectrum of graphite. *J. Chem. Phys.*, 1970, **53**(3), 1126–1130.
28. Wada, N. and Solin, S. A., Raman efficiency measurements of graphite. *Physica B & C*, 1981, **105**(1–3), 353–356.
29. Nikiel, L. and Jagodzinski, P. W., Raman-spectroscopic characterization of graphites—a reevaluation of spectra/structure correlation. *Carbon*, 1993, **31**(8), 1313–1317.
30. Bhushan, B., *Principles and Applications of Tribology*. John Wiley & Sons, NY, 1999.
31. Savage, R. H., Graphite lubrication. *J. Appl. Phys.*, 1948, **19**(1), 1–10.
32. Nakamura, M., Hirao, K., Yamauchi, Y. and Kanzaki, S., Tribological properties of unidirectionally aligned silicon nitride. *J. Am. Ceram. Soc.*, 2001, **84**(11), 2579–2584.
33. Fischer, T. E. and Tomizawa, H., Interaction of tribochemistry and microfracture in the friction and wear of silicon nitride. *Wear*, 1985, **105**, 29–45.